X-ray photoelectron diffraction and Auger electron diffraction from $TiO_2(100)$

P. J. Hardman, P. L. Wincott, and G. Thornton*
Surface Science Research Centre and Chemistry Department, University of Manchester, Manchester M13 9PL, United Kingdom

A. P. Kaduwela and C. S. Fadley
Materials Science Division, Lawrence Berkeley National Laboratory, Berkeley, California, 94720

(Received 18 August 1998)

Full-hemispherical x-ray photoelectron (Ti$2p$/O$1s$) and x-ray stimulated Auger electron (Ti$L_3M_{23}M_{23}$/O KVV) intensity distributions have been measured from $TiO_2(100)1\times1$ at relatively high-angular resolution ($\pm1.8°$). The results are compared with theoretical calculations using a multipole *R*-factor analysis. Multiple scattering up to fifth order and a slab thickness of ~16 Å are needed to obtain optimum agreement with experimental photoelectron distributions. We also investigate the contribution of the final state wave function in the Auger-electron diffraction patterns and show that it is possible to determine the symmetry of the final state angular momenta for oxides such as TiO_2. Both the x-ray photoelectron diffraction and the x-ray stimulated Auger intensity distributions are found to be insensitive to details of the surface structure. [S0163-1829(99)03531-6]

I. INTRODUCTION

For metals and elemental semiconductors it has been widely demonstrated that x-ray photoelectron diffraction (XPD) data are dominated by forward scattering processes at kinetic energies greater than 500 eV.[1,2] In many cases the analysis of such XPD data has been accomplished with simple single scattering calculations,[1,2] which allow a rapid comparison of theory and experiment.[1–3] These generally yield good agreement between experimental diffraction patterns and single scattering (SS) theory. This arises for two reasons. First, the atoms are generally strong scatterers, due to their relatively large atomic masses $Z\geqslant14$. This gives rise to strong forward scattering intensities, thus minimizing the effects of multiple scattering (MS) on the experimental patterns. Secondly, the relatively large acceptance angles ($\geqslant\pm6°$) that have been employed have the effect of broadening the observed diffraction features, averaging out fine structure due to multiple scattering as well as long-range scattering.

As for metal-oxide surfaces, XPD has been used to study both thin films grown on metals[4,5] and single crystal substrates.[6–8] Both clean[9–14] and adsorbate covered[15] oxide surfaces have been investigated. For example, the surface termination and relaxations of polar ZnO (0001) surfaces were determined by comparison with single scattering cluster calculations.[13,14] Recent studies of $TiO_2(110)$ (Refs. 6 and 9) have employed angle-scanned photoelectron diffraction to collect full-hemispherical diffraction patterns for emission from the Ti $2p$ core level. Sambi *et al.*[6] compared their data to single-scattering calculations, which provided good agreement with the position of the main forward focusing maxima observed in the experimental data. More recently, there have been studies of formic acid on $TiO_2(110)$.[15]

In contrast to XPD, Auger electron diffraction has been less frequently employed in the study of surfaces. Much of the early experimental work on Auger electron diffraction (AED) assumed that the outgoing Auger electron had an isotropic distribution and could simply be treated as an *s* wave in theoretical calculations.[16,17] However, more recent results have shown that the final state of the Auger electron should be taken into account if the best agreement between theory and experiment is to be obtained.[18,19] This requirement to take the source wave character into account becomes even more important at lower kinetic energies, i.e., <100 eV, as has been demonstrated for metal surfaces such as Cu(001), Al(001), and Pt(111).[19] The analysis of AED is further complicated by the nature of the multielectron Auger process, which involves coupling of the electron initial states, giving various possible final state angular momentum distributions.[20] Theoretical calculations of the diffraction patterns are needed to fully utilize these Auger data.

Here we employ the $TiO_2(100)$ surface as a model system with which to explore the observed XPD and AED patterns from an oxide surface recorded at relatively high-angular resolution ($\pm2°$). This surface has previously been extensively studied using a variety of techniques,[21] and recent scanning tunneling microscopy results of the 1×1 phase[22] are consistent with the structure expected on the basis of Tasker's rules.[23] This is shown in Fig. 1. The effect of angular resolution on XPD has been demonstrated experimentally by Pathey and Bullock for $TiO_2(110)$.[9] They showed that experimental features become sharper as the acceptance angle is reduced. In similar experiments we have also observed a significant (fivefold) enhancement in the anisotropy of the diffraction patterns as the angular resolution is increased.[24] This increase in anisotropy can be employed for measurements where the anisotropy would otherwise be expected to be small, such as those recently reported by Greber *et al.* for O on Rh(111).[25] For $TiO_2(100)$ we find that to successfully model our high-angular resolution data we must employ multiple scattering simulations.

II. EXPERIMENTAL DETAILS

The measurements were performed in a UHV chamber that has been described elsewhere.[26] Photoelectron and Au-

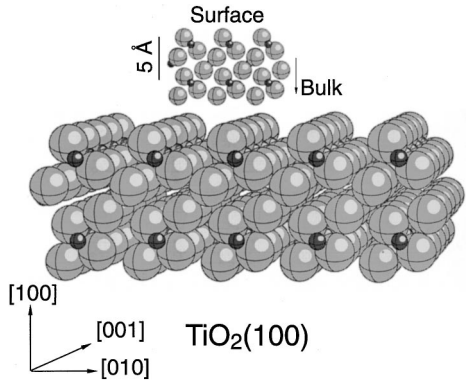

FIG. 1. Model of the bulk-terminated $TiO_2(100)1\times1$ surface expected on the basis of Tasker's rules (Ref. 23). Large (small) spheres represent O (Ti) atoms scaled to the appropriate ionic radii (Ref. 40).

ger electron spectra, and associated diffraction patterns were recorded at room temperature using a VSW/Omicron EA125 analyzer with a five-channeltron detection system and unpolarized Mg $K\alpha$ ($h\nu=1253.6$ eV) radiation. The data were collected with an analyzer pass energy of 20 eV and the analyzer lens in low-magnification mode. This gives an x-ray source limited energy resolution $\Delta E=0.7$ eV [full width at half maximum (FWHM)] and an angular resolution $\Delta\theta=\pm2°$ (FWHM) for all the measurements. The x-ray source was mounted 70° off normal, and 45° out of plane, with respect to the analyzer-surface normal (which was in the horizontal plane). During the experiments the chamber base pressure was $\leqslant2\times10^{-10}$ mbar.

The rutile TiO_2 sample was cut and polished to within 0.1° of the (100) plane, as checked by Laue diffraction. To prevent sample charging effects, the sample was prereduced such that it was blue gray in color, indicating an *n*-type carrier concentration of about 10^{18} cm^{-3}.[27] The sample was cleaned *in situ* by 500 eV Ar^+ sputtering and subsequent annealing to 870 K. This cycle was repeated until contaminant levels (C,S,K,Cl) were less than 1% as judged by Auger electron spectroscopy (AES). The 1×1 nominally stoichiometric surface was formed by annealing the clean sample in 1×10^{-6} mbar O_2 (99.985%; BOC Research Grade) at 870 K for 30 min, and cooling to 400 K in O_2. This procedure restored the surface to close to stoichiometric, as judged by the lack of a Ti $2p$ shoulder in photoemission,[28] and the presence of a good 1×1 low energy electron diffraction (LEED) pattern.

The sample was mounted on a modified sample manipulator (VG Omniax) capable of $>360°$ azimuthal rotation with an angular precision of $\pm0.5°$ in both polar ($\theta=0$ at normal emission) and azimuthal angle (ϕ, defined with respect to the [001] direction of the substrate). During azimuthal rotation the sample alignment (polar angle) was checked using laser reflection from the sample surface, and it was found to be less than $\pm0.5°$ over the full 360°. The sample normal ($\theta=0°$) was determined using the (0,0) LEED beam. The azimuthal alignment was initially determined by LEED, but further fine adjustments were made using the symmetry of fine-step (1°) azimuthal scans.

The room-temperature diffraction patterns were obtained by rotating the sample in front of the fixed analyzer and collecting azimuthal scans for a range of polar angles. Two modes of data collection were used. The first was a simple integration of the signal collected over all five channeltrons centered on the peak of interest. This method is very similar to that used by Patthey and Bullock for $TiO_2(110)$.[9] The second method involved recording a full-electron distribution curve (EDC) at each angular data point, and then subsequently integrating the area under the peak after removing a linear background. The two sets of results were found to be very similar. However, the second method is favored as it averages the data from all five channeltrons, thus reducing the effect of any changes in the channeltron sensitivity during the data collection time (ca. 12 hr). The EDC's for the Ti $2p$ peak contained both the $2p_{\frac{3}{2}}$ and the $2p_{\frac{1}{2}}$ contributions. No contamination was observed on the sample using AES after the end of scans.

III. COMPUTATIONAL DETAILS

The calculations were performed using the multiple scattering code described by Kaduwela, Friedman, and Fadley.[29] This cluster-based method allows multiple scattering to be included up to 10th order and can treat photoelectron emission from any initial state with full final state interference. The radial dipole matrix elements for the various kinetic energies employed were calculated using the method described by Goldberg, Fadley, and Kono.[30]

As a starting point for our calculations we used the unrelaxed $TiO_2(100)1\times1$ structure shown in Fig. 1. To obtain the best agreement with experiment it was necessary to include Ti emitters from eight layers into the surface. This resulted in clusters of up to 250 atoms and an effective sampling depth for these calculations of up to 16.83 Å . The inelastic attenuation length was set to 10 Å and the inner potential used was 10 eV, which are typical values for oxides.[31–33] It was found that the results were insensitive to changes of the order $\pm50\%$ in the values of the inner potential or the attenuation length. The scattering phase shifts were calculated in the framework of the partial wave method within a muffin-tin approximation using the MUFPOT program.[34] Angular broadening of the electron emission direction to match the finite angular acceptance ($\pm1.8°$) of the analyzer was also included in the simulations. To compare the experimental results with the theoretical calculations we used a multipole *R* factor, which has previously been described by Fasel *et al.* for work on $c(2\times2)$-Na on Al(001).[35]

IV. EXPERIMENTAL RESULTS

The full-hemispherical diffraction plots for $TiO_2(100)$ 1×1 using Ti $L_3M_{23}M_{23}$ Auger ($KE=375$ eV), O KVV Auger ($KE=508$ eV), O $1s$ ($KE=719$ eV), and Ti $2p$ ($KE=795$ eV) are shown in Fig. 2. Each plot comprises 3600 data points distributed in 3° steps in θ and ϕ. The azimuthal step was kept constant over the whole plot so as to allow easier comparison with theory. The center of each plot corresponds to the surface normal ($\theta=0$), with radial sections representing polar scans and circular sections representing azimuthal scans. The relative intensity is indicated by the scale ranging from black=minimum to white=maximum. The data have been fourfold averaged by reflecting across

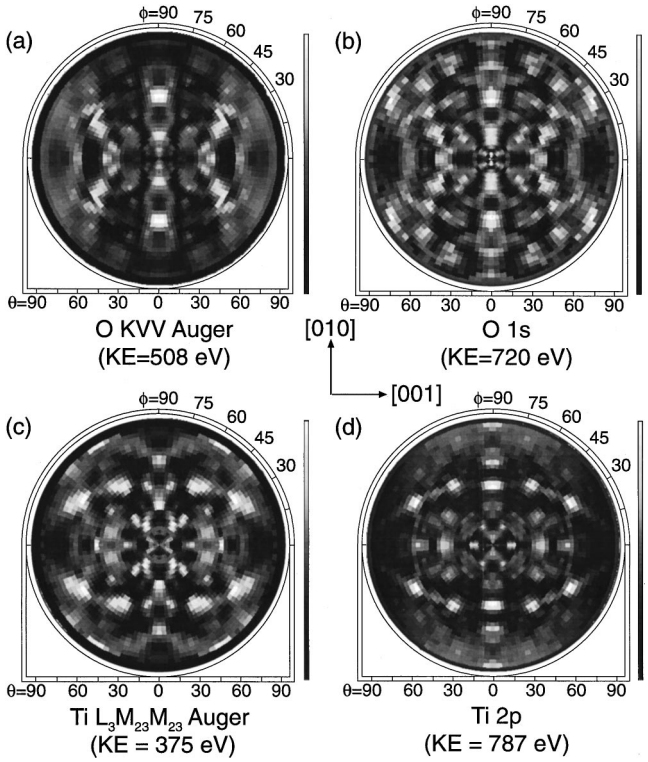

FIG. 2. Experimental photoelectron (Mg $K\alpha$) and Auger electron diffraction data ($h\nu = 1253.6$ eV) from $TiO_2(100)$. (a) O KVV Auger $KE = 508$ eV. (b) O $1s$ $KE = 720$ eV. (c) Ti $L_3M_{23}M_{23}$ Auger $KE = 375$ eV. (d) Ti $2p$ $KE = 787$ eV. Each plot, consisting of 3600 data points, has been normalized as follows. First the intensity of each azimuthal scan was set to range between zero and unity to remove any polar angle emission dependent effects. Then the average intensity of each azimuthal scan was set to equal zero, making each azimuth vary around zero. Finally the whole plot is set to range from zero to one. (θ and ϕ steps $= 3°$. $\theta = 0°$ at normal emission, ϕ is defined with respect to the [001] direction).

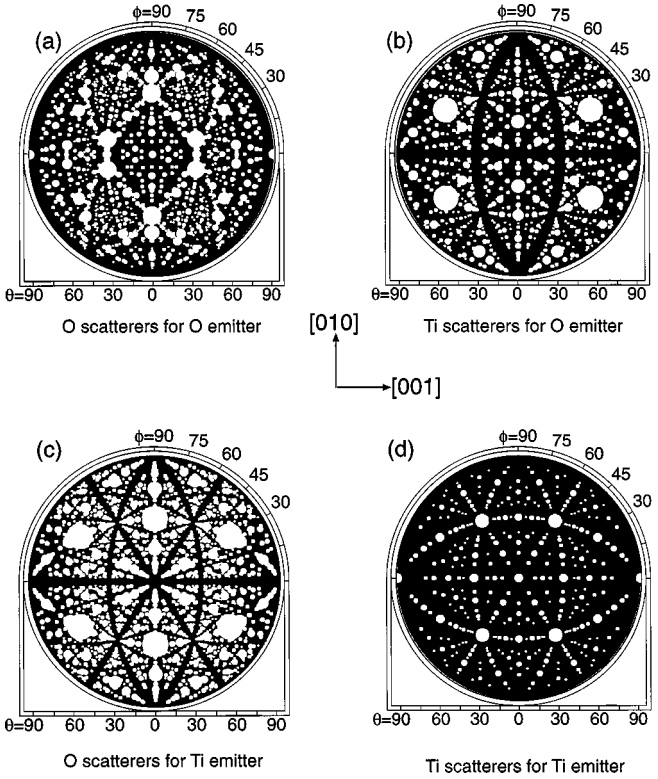

FIG. 3. Schematic representations of the scattering directions for Ti and O emitters in $TiO_2(100)$. The patterns are generated by employing the clusters used to carry out the full theoretical multiple scattering calculations. One atom is chosen as the emitter with every other atom in the cluster considered as a scatterer. For each emitter-scatterer combination a circle is drawn centered on the emitter-scatterer direction. The size of the circle is inversely proportional to the emitter-scatterer distance. We consider the four possible scatterer-emitter combinations: (a) O-O; (b) Ti-O; (c) O-Ti; and (d) Ti-Ti. Note that the largest spots appear in (b) and (c) because they have the smallest emitter-scatterer distances.

the [001] and [010] azimuths, and normalized so that the average intensity at each polar angle equals zero.[35] The averaging across the [001] and [010] azimuths serves only to remove some minor experimental variations observed in the raw data, since in general the agreement between the averaged and raw data is excellent. It is immediately obvious that the data from Ti emitters are quite different from the data from O emitters, being due to the difference in the local atomic arrangement around the Ti and O atoms in TiO_2.

V. DISCUSSION

The most obvious features in the XPD patterns of Fig. 2 are the bright areas or ''spots'' that are attributed to forward scattering (also referred to as forward focusing) from neighboring atoms. These are surrounded by fine structure due to higher order interference and forward scattering from more distant neighbors. Interatomic directions in the crystal can be determined from these forward scattering spots, since at these kinetic energies the greatest intensity is found in the forward scattering direction when the emitter, scatterer, and detector are aligned.[1,2,19] The simplest way to do this is to compare the experimental results with the plots shown in Fig. 3. These plots simulate the directions in the crystal where either Ti or O scatterers lie with respect to either a Ti or O emitter. These directions are represented by circles centered on the scattering direction, where the circle radius is inversely proportional to the emitter scatterer separation. For this reason, the largest spots in plots 3(b) and 3(c) are due to scattering off the nearest neighbors of the opposite element. The patterns for Ti scatterers are much simpler than those for O scatterers since in rutile TiO_2 there is only one type of Ti site compared to three sites for O. This is due to the distorted octahedral environment of Ti in rutile.[32]

By comparing these simple scattering plots with the experimental results, we find that all of the major features, and also many of the weaker features in the experimental data can be assigned to forward scattering processes in the crystal. This agreement is especially good between the Ti $2p$ and Ti $L_3M_{23}M_{23}$ Auger data and the Ti emitter simulations, but less so for the O $1s$ and O KVV Auger results. One reason for the poorer agreement might be the larger number of possible emitter-scatterer directions for O compared to Ti. This would decrease the relative contrast of the experimental data.

In the next section we focus on the photoemission results for the O $1s$ and Ti $2p$ emitters. The results of SS and MS (up to fifth order) calculations for O $1s$ and Ti $2p$ emitters are shown in Fig. 4. The results have been normalized in the

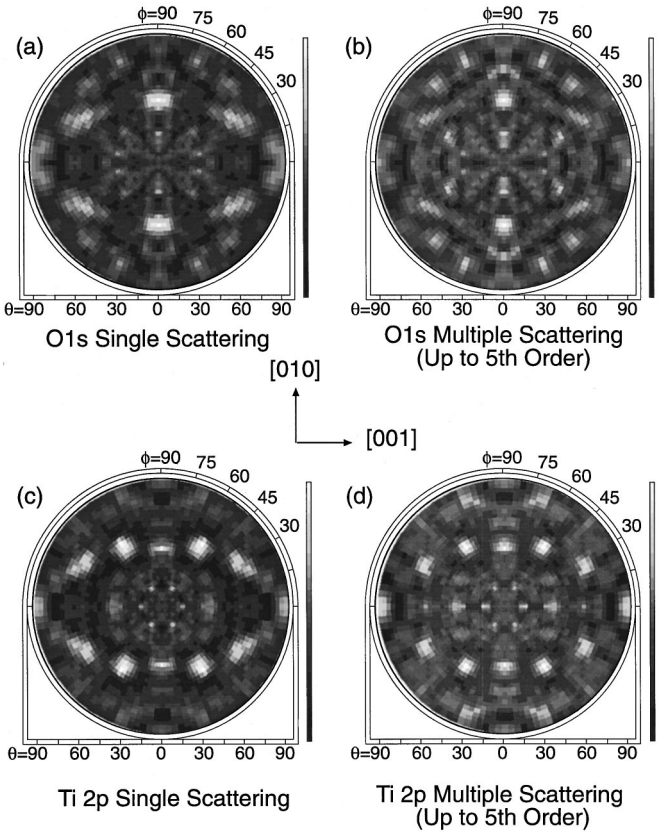

FIG. 4. Results of theoretical calculations for $TiO_2(100)$ O 1s and Ti 2p Mg $K\alpha$ photoelectron diffraction with both single scattering (SS) and fifth-order multiple scattering (MS). The θ and ϕ steps are the same as in Fig. 2. (a) O1s SS; (b) O1s MS; (c) Ti 2p SS; and (d) Ti 2p MS. The Ti 2p data contains contributions from Ti atoms up to 16.82 Å into the bulk. The O 1s data contain contributions from O atoms up to 12.23 Å into the bulk. These data have been normalized using the same procedure as outlined for the experimental data shown in Fig. 2.

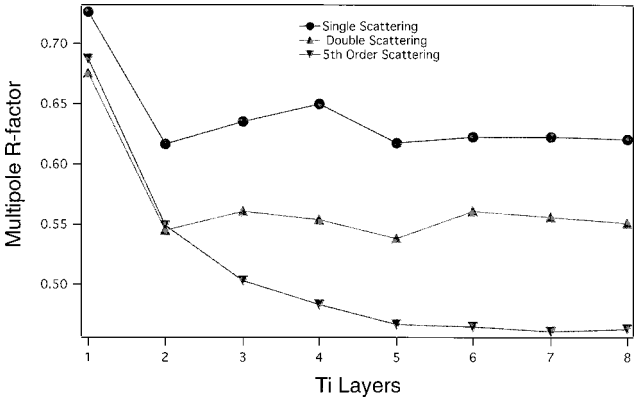

FIG. 5. Multipole R factors (Ref. 35), which compare Ti 2p Mg $K\alpha$ photoelectron calculations using single scattering, double scattering, and fifth-order multiple scattering as a function of Ti layers in the calculations with the Ti 2p experimental data shown in Fig. 2.

same way as the experimental data to allow a direct comparison to be made. The calculations comprise a summation of results for all emitters up to the 12th O layer (12.23 Å) into the bulk, for O 1s emission, and up to the eighth Ti layer (16.83 Å) for Ti 2p emission. We were unable to increase the emitter depth above these values due to memory constraints on the cluster size, but we note that the clusters used represent emission from layers up to 1.5 times the attenuation length used in the calculations (10 Å). Looking first at the Ti 2p data we find that all of the main features of the experiment have been reproduced by the theoretical calculations with both SS and MS. In the single scattering calculations the relative intensity of the forward focusing peaks have been overestimated compared with experiment,[29] and we find a much better agreement with the results of MS calculations as discussed below. The attenuation of the experimental forward focusing features, compared with the SS theory, is partly due to defocusing along chains of atoms,[29] and also to scattering into paths other than the forward scattering direction.

We have used the multipole R factor described by Fasel *et al.*[35] to compare the results of our calculations for increasing numbers of Ti layers for both SS, double scattering (DS), and fifth order MS. From the R-factor results shown in Fig. 5, we find that adding a second Ti layer results in a decrease of the R factor for each of the theoretical models, with the DS and MS results giving the same R factors. As more layers are added, the SS and DS R factors remain about the same while the MS values fall further and finally reach a plateau at 7-8 layers, which was the limit of our calculations. A selection of azimuthal scans from the Ti 2p data in Fig. 2(d) are shown in Fig. 6. They compare the experiment with SS and MS calculations and show that overall the agreement is very good. The azimuthal scan for $\theta=36°$ is a good example of how the SS theory overestimates the intensity of the forward scattering peaks at $\phi=90°$ and $\phi=270°$, and how including MS attenuates this feature to give a much better agreement with experiment.

If we now turn to the O 1s data, and compare the results in Figs. 2(b) and 4(a) and 4(b) we find essentially the same effect of including MS in the XPD calculations as for the Ti 2p results. For example, the feature at $\theta=45°$ along the [010] direction is much more intense in SS than it is with MS or experiment. This can also be observed in the azimuthal scans shown in Fig. 7. The data for $\theta=33°$ and 60° show that including MS leads to an attenuation of the peaks and hence a much better agreement with the experiment. In other areas, for instance the features at $\phi°=69$, 111, 249, and 291 in the $\theta=33°$ data shown in Fig. 7(c), can be assigned to MS on the basis of their absence in the SS simulation.

In our calculations we also considered a surface Ti-terminated surface with the top layer of O atoms removed as a possible cause for the mismatch between theory and experiment. We found that this did not affect the overall results of the calculations, since most of the electrons undergoing diffraction originate from deeper layers, with the surface playing only a small part in determining their final emission direction. We therefore conclude that these experiments are insensitive to the surface structure, due to the high-kinetic energy of the electrons involved and the large contribution from deeper laters. This does not mean that XPD is incapable of providing information about oxide-surface structure. If lower kinetic energies ($\leqslant$200 eV) are used or methods are employed to isolate the surface contribution, such as surface

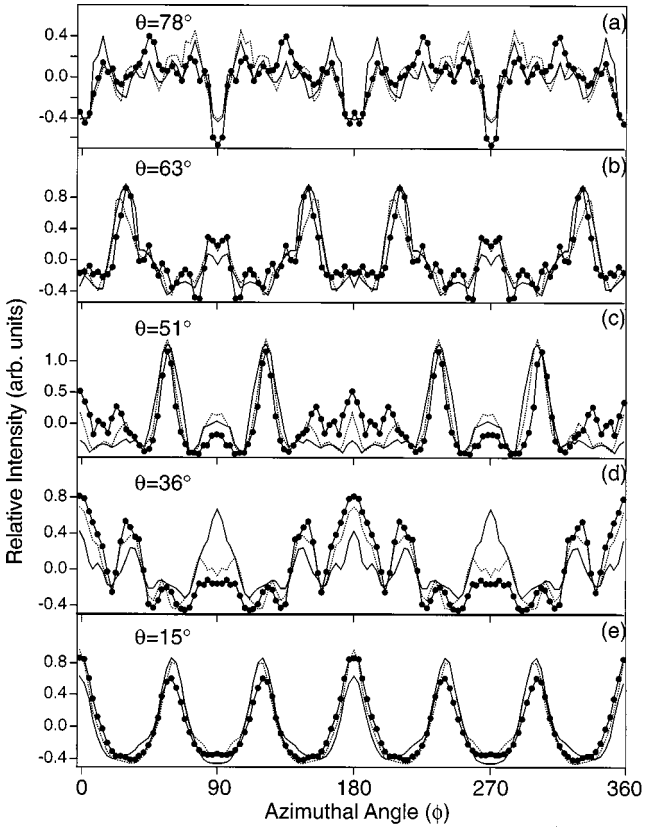

FIG. 6. Selected Mg $K\alpha$ Ti $2p$ photoelectron azimuthal scans. Each scan has been normalized as follows. First the intensity of each azimuthal scan was set to range between zero and unity to remove any polar angle emission effects. Then the average intensity of each azimuthal scan was set to equal zero. Solid (dashed) lines represent single (multiple) scattering calculations and the experimental data are represented as small circles joined by a solid line. At normal emission $\theta=0$.

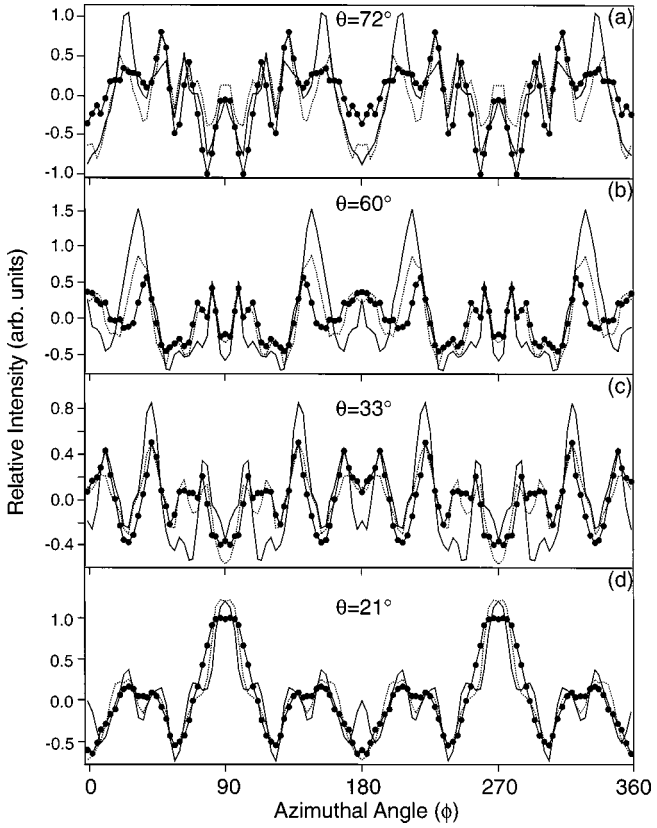

FIG. 7. As Fig. 6, but for O $1s$.

core-level shifts, then much useful information can be gained.[11]

Now we turn to the Auger electron diffraction data shown in Figs. 2(a) and 2(c). At first glance these data are quite similar to the corresponding photoelectron diffraction data. However, on closer examination one finds that in general the forward focusing maxima are broader and that the surrounding fine structures is less sharply defined. Many of these changes can be attributed to the lower kinetic energy of the emitted electrons, and the consequential increase in multiple scattering and weaker forward focusing. Another factor that must be taken into account in Auger emission, as in photoemission, is the angular momentum of the outgoing electron wave. Early experiments assumed that Auger electrons could be treated as s waves with an isotropic angular distribution,[16,17] but more recent work has shown that it is important to take the angular momentum of the outgoing Auger electron wave into account.[18,19]

To take the Auger electron angular momentum into account, we have performed calculations for electrons with different values of the angular momentum quantum number l. In Fig. 8 we show the results of fifth order MS calculations for Ti $L_3M_{23}M_{23}$ Auger electrons with different values of l from 0 to 3. The results of the multipole R-factor comparison for s, p, d and f final state waves are shown in the lower section of Fig. 9(a). From the R factors, we find a minimum for electrons emitted with d-wave character ($l=2$). A more refined approach takes account of the known origin (Ti $2p$,Ti $3p$) of this Auger process. We can use the following angular momentum relationships to predict the possible angular momentum of the Auger electron[18]

$$|l_i-|l_j-l_k||\leqslant l\leqslant l_i+l_j+l_k,$$

and

$$l_i+l_j+l_k+l=\text{even},$$

where l_i, l_j, and l_k represent the angular momenta of the initial core hole and final-state holes, respectively. For this transition, $l_i=1$, $l_j=1$, and $l_k=1$. This gives either $1\leqslant l\leqslant 3$ and $3+l$ must be even so l is either 1 or 3. This gives a final state angular momentum of either $l=1$, i.e., a p wave or $l=3$, i.e., an f wave. This leads us to consider a mixed final state angular momentum for the Auger electron comprising both p waves and f waves, which we have compared with experiment. To do this we take linear combinations of the p- and f-wave calculations and compare them with the experimental data. We find that the minimum in the multipole R factor occurs when we combine a 50% p-wave component with a 50% f-wave component.

Turning now to the O KVV data, the results of the R-factor comparisons for different angular momenta are shown in Fig. 9(b). A comparison of pure s, p, and d waves with experiment yields the R factors in the lower graph. Here, we find a minimum for electrons emitted with d-wave

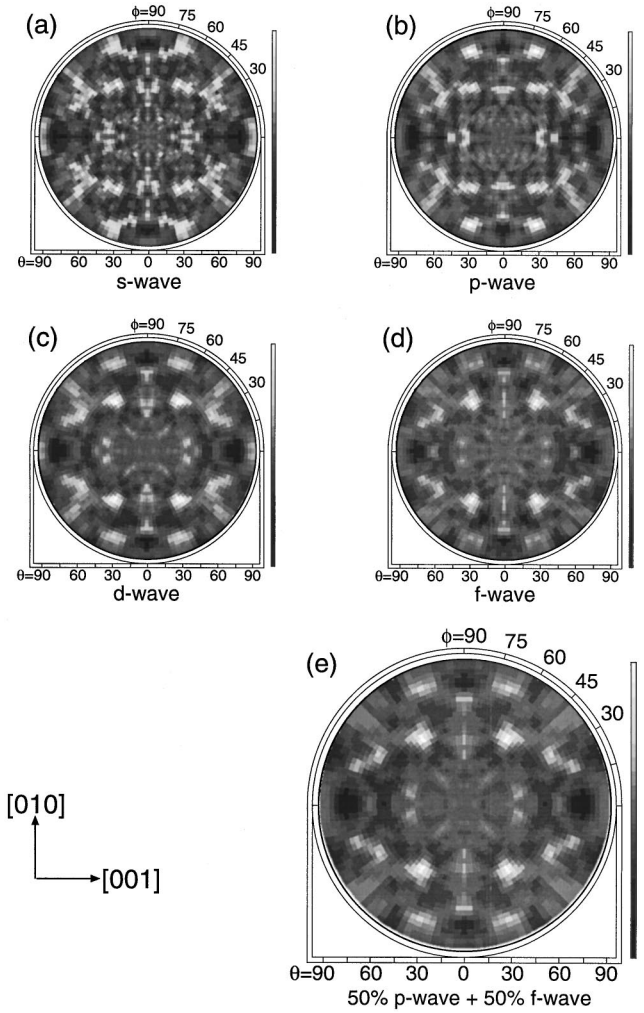

FIG. 8. Theoretical diffraction patterns due to the 375-eV Ti $L_3M_{23}M_{23}$ Auger electron emission from $TiO_2(100)1\times1$ for various final state angular momentum: (a) *s*-wave emitter; (b) *p*-wave emitter; (c) *d*-wave emitter; and (d) *f*-wave emitter. The final plot (e) shows the best fit with experiment found by mixing a 50% *p* component with a 50% *f* component.

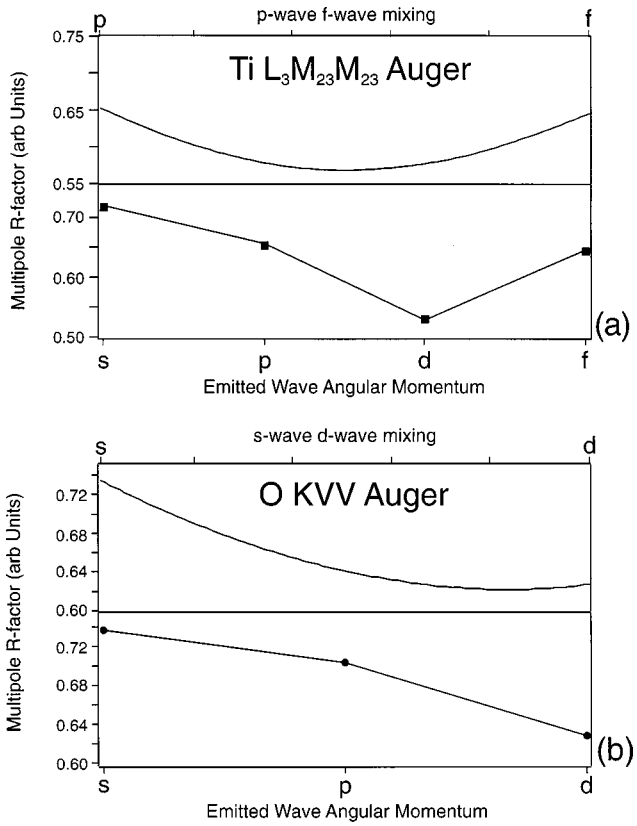

FIG. 9. *R*-factor plots for the comparison of Auger electron diffraction experiments and calculations. (a) The results for Ti $L_3M_{23}M_{23}$ with the lower graph showing a minimum in the *R* factor for *d* waves when only one emitted angular momentum is included. The results for a mixed p/f final state are shown in the upper graph where a minimum occurs at a 50% *p* component and 50% *f* component. (b) The results for O KVV with the lower graph showing a minimum in the *R* factor for *d* waves when only one emitted angular momentum is included. The results for a mixed s/d final state are shown in the upper graph where a minimum occurs with an 18% *s* component and an 82% *d* component.

character ($l=2$). However, an analysis of the situation for the O KVV Auger angular momentum, where $l_i=0$, $l_j=1$, and $l_k=1$, indicates that l is either $l=0$, i.e., an *s* wave or $l=2$, i.e., a *d* wave. From the results of the linear combination of these two angular momentum final states we find that the best agreement with experiment is for 82% *d* wave and 18% *s* wave.

In order to evaluate the analysis above, we make a comparison with the experimentally determined values for the final state angular momenta of the outgoing electrons by using the tables of Asaad[36] and McGuire,[37] and the method outlined by Aberdam *et al.*[38] This predicts that the Ti $L_3M_{23}M_{23}$ Auger comprises 51.5% *p* and 48.5% *f* character, which is in excellent agreement with the experimental result. We were unable to perform a similar calculation for the O KVV Auger transition since we could not locate tabulated values for this transition. However, the s/d ratio derived from experiment is biased towards a *d* wave, consistent with that expected on the grounds of general arguments.[39]

VI. CONCLUSIONS

We have examined XPD patterns from $TiO_2(100)1\times1$ and compared them with multiple scattering calculations. We find that multiple scattering is important in modeling the diffraction patterns, at the higher resolution employed, where single scattering calculations overestimate the intensity and width of features. It is equally important to use large clusters in the final calculations, as layers up to at least 16 Å can contribute to the experimental data. Furthermore, we have been able to determine the angular momentum of the outgoing Auger electrons, which are in excellent agreement with theoretically determined values.[36–38] This further demonstrates that it is important to take into account the symmetry of the outgoing wave in any theoretical treatment of Auger electron diffraction.[18,19] We find that these results are insensitive to the surface structure. This is not surprising given the high-kinetic energy of the electrons measured and hence their long mean-free path. However, this paper forms the basis for further XPD studies of oxide surfaces at high-angular resolution, and demonstrates the viability of calculations for such systems.

ACKNOWLEDGMENTS

The authors would like to acknowledge Dr. D. Aberdam for kindly providing copies of research reports and Mr. I. Brookes for implementing and testing the multipole *R*-factor code. This work was funded by EPSRC (UK) with additional support from NATO. The development of the multiple scattering code was supported by the U.S. Department of Energy, Basic Energy Sciences, Materials Sciences Division (Contract No. DOE-AC03-76F00098).

*Author to whom correspondence should be addressed.

[1] C.S. Fadley, in *Synchrontron Radiation Research: Advances in Surface Science*, edited by R.Z. Bachrach (Plenum, New York, 1992), Chap. 11.
[2] W.F. Egelhoff, Jr., Crit. Rev. Solid State Mater. Sci. **16**, 213 (1990).
[3] M. Sagurton, E.L. Bullock, and C.S. Fadley, Surf. Sci. **182**, 287 (1987).
[4] Y.J. Kim, C. Westphal, R.X. Ynunza, and H.C. Galloway, Phys. Rev. B **55**, 13 448 (1997).
[5] A. Atrei, U. Bardi, and G. Rovida, Surf. Sci. **391**, 216 (1997).
[6] M. Sambi, G. Sangiovanni, G. Granozzi, and F. Parmigiani, Phys. Rev. B **55**, 7850 (1997).
[7] M. Sambi, E. Pin, G. Sangiovanni, L. Zaratin, G. Granozzi, and F. Parmigiani, Surf. Sci. Lett. **349**, L169 (1996).
[8] M. Sambi, G. Sangiovanni, G. Granozzi, and F. Parmigiani, Phys. Rev. B **54**, 13 464 (1996).
[9] L. Patthey and E.L. Bullock, J. Electron Spectrosc. Relat. Phenom. **83**, 99 (1997).
[10] B. Hermsmeier, J. Osterwalder, D.J. Friedman, B. Sinkovic, T. Tran, and C.S. Fadley, Phys. Rev. B **42**, 11 895 (1990).
[11] P.J. Hardman, N.S. Prakash, C.A. Muryn, G.N. Raikar, A.G. Thomas, A.F. Prime, G. Thornton, and R.J. Blake, Phys. Rev. B **47**, 16 056 (1993).
[12] C. Scharfschwerdt, T. Liedtke, M. Neuman, T. Straub, and P. Steiner, Phys. Rev. B **48**, 6919 (1993).
[13] M. Sambi, G. Granozzi, E.A. Rizzi, M. Casarin, and E. Tondello, Surf. Sci. **319**, 149 (1994).
[14] M. Galeotti, A. Atrei, U. Bardi, G. Rovida, M. Torrini, E. Zannazi, A. Santucci, and A. Klimov, Chem. Phys. Lett. **222**, 349 (1994).
[15] S.A. Chambers, S. Thevuthasan, Y.J. Kim, G.S. Herman, Z. Wang, E. Tober, R. Ynzunza, J. Morais, C.H.F. Peden, K. Ferris, and C.S. Fadley, Chem. Phys. Lett. **267**, 51 (1997).
[16] M.-L. Xu and M.A. Van Hove, Surf. Sci. **207**, 215 (1989).
[17] D.G. Frank, N. Batina, T. Golden, F. Lu, and A.T. Hubbard, Science **247**, 182 (1990).
[18] D.K. Saladin, G.R. Harp, and B.P. Tonner, Phys. Rev. B **45**, 9629 (1992).
[19] L.J. Terminello and J.J. Barton, Science **251**, 1218 (1991); T. Greber, J. Osterwalder, D. Naumovic, A. Stuck, S. Hüfner, and L. Schlapbach, Phys. Rev. Lett. **69**, 1947 (1992); T. Greber, J. Osterwalder, S. Hüfner, and L. Schlapbach, Phys. Rev. B **45**, 4540 (1992); Y.U. Idzerda and D.E. Ramaker, Phys. Rev. Lett. **69**, 1943 (1992).
[20] D. Chattarji, *The Theory of Auger Transitions* (Academic, London, 1976).
[21] V. E. Henrich and P. A. Cox, *The Surface Science of Metal Oxides*, (Cambridge University Press, Cambridge, 1994).
[22] H. Raza, C.L. Pang, S.A. Haycock, and G. Thornton, Appl. Surf. Sci. **140**, 271 (1999).
[23] P.W. Tasker, J. Phys. C **12**, 4977 (1979).
[24] Results from azimuthal O 1*s* scans of $TiO_2(110)$ (Mg $K\alpha, \theta = 45°$) at angular resolutions of $\pm 8°$, $\pm 4°$, and $\pm 2°$ give measured anisotropies of 7%, 26%, and 46%, respectively.
[25] T. Greber, J. Wider, E. Wetli, and J. Osterwalder, Phys. Rev. Lett. **81**, 1654 (1998).
[26] P.L. Wincott, N.B. Brookes, D.S.-L. Law, G. Thornton, and G.C. King, J. Phys. E **22**, 42 (1988).
[27] D.C. Croynmeyer, Phys. Rev. **87**, 876 (1952).
[28] G. Rocker and W. Göpel, Surf. Sci. **181**, 530 (1987).
[29] A.P. Kaduwela, D.J. Friedman, and C.S. Fadley, J. Electron Spectrosc. Relat. Phenom. **57**, 223 (1991).
[30] S.M. Goldberg, C.S. Fadley, and S. Kono, J. Electron Spectrosc. Relat. Phenom. **21**, 285 (1981).
[31] P.J. Hardman, G.N. Raiker, C.A. Muryn, G. van der Laan, P.L. Wincott, G. Thornton, D.W. Bullett, and P.A.D.M.A. Dale, Phys. Rev. B **49**, 7170 (1994).
[32] C.G. Mason, S.P. Tear, T.N. Doust, and G. Thornton, J. Phys.: Condens. Matter **3**, S97 (1991).
[33] M.P. Seah and W.A. Dench, Surf. Interface Anal. **1**, 2 (1979).
[34] J.B. Pendry, *Low Energy Electron Diffraction* (Academic, London, 1974).
[35] R. Fasel, A. Aebi, J. Osterwalder, L. Schlapbach, R.G. Agostino, and G. Chiarelo, Phys. Rev. B **50**, 14 516 (1994).
[36] W.N. Assad, Nucl. Phys. **44**, 399 (1963).
[37] E.J. McGuire, Sandia Laboratories, Research Report No. SC-RR-710075, 1971 (unpublished).
[38] D. Aberdam, R. Baudoing, E. Blanc, and C. Gaubert, Surf. Sci. **71**, 279 (1978).
[39] D. Ramaker (private communication).
[40] R.D. Shannon, Acta Crystallogr., Sect. A: Cryst. Phys., Diffr., Theor. Gen. Crystallogr. **32**, 751 (1976).